Mechanistic Investigation of Medium-Chain Fatty Acyl-CoA Dehydrogenase Utilizing 3-Indolepropionyl/Acryloyl-CoA as Chromophoric Substrate Analogues†

Jeffrey K. Johnson, Zhi-Xin Wang, and D. K. Srivastava*

Biochemistry Department, North Dakota State University, Fargo, North Dakota 58105

Received April 21, 1992; Revised Manuscript Received August 10, 1992

ABSTRACT: The CoA derivative 3-indolepropionyl-CoA (IPCoA) serves as a competent pseudosubstrate for the medium-chain fatty acyl-CoA dehydrogenase (MCAD)-catalyzed reaction. The reaction product *trans*-3-indoleacryloyl-CoA (IACoA) exhibits a characteristic UV–vis absorption spectrum with λ_{max} = 367 nm and ϵ_{367} = 26 500 M^{-1} cm^{-1}. The chromophoric nature of IACoA allows us to measure the direct conversion of substrate to product (at 367 nm) without recourse to absorption signals for either the enzyme-bound flavin or the coupling electron acceptors, as well as probe the enzyme site environment. The interaction of IACoA with medium chain fatty acyl-CoA dehydrogenase (MCAD)-FAD is characterized by resultant (spectra of the mixture minus the individual components) absorption peaks at 490, 417, and 355 nm. These absorption peaks increase in magnitude as the pH of the buffer media decreases. Transient kinetic analysis for the interaction of MCAD–FAD with IACoA suggests that the formation of the enzyme–IACoA complex proceeds in two steps. The first (fast) step involves the formation of an E–IACoA collision complex, which

$$E + IACoA \underset{K_c}{\rightleftharpoons} E\text{–}IACoA \underset{k_{-2}}{\overset{k_2}{\rightleftharpoons}} E^*\text{–}IACoA$$

is isomerized (concomitant with changes in the protein structure) to an E*–IACoA complex in the second (slow) step. We have studied the effect of pH on K_c, k_2, and k_{-2}. While K_c shows practically no dependence on pH (within a 2-fold variation between pH 6.0 and 9.5), k_2 and k_{-2} show a strong dependence on pH. Both k_2 and k_{-2} exhibit a sigmoidal dependence on the pH of the buffer media, with pK_a's of 7.53 and 8.30, respectively. In accordance with the model presented herein, the pK_a of 7.53 represents an enzyme site group which is involved in the interaction with IACoA within the E–IACoA collision complex. This pK_a is perturbed to 8.30 upon isomerization of the collision complex. The pH-dependent changes in k_2 and k_{-2} are such that the equilibrium distribution between E–IACoA and E*–IACoA is favored to the latter complex (by about 20-fold) at lower pH than at higher pH. A cumulative account of the spectral, kinetic, and thermodynamic properties of the enzyme–IACoA complexes has allowed us delineate the microscopic pathway by which the E–IACoA isomerization (presumably via protein conformational changes) is coupled to the proton equilibration steps.

The mammalian β-oxidative pathway of fatty acids proceeds via a sequence of enzymatic steps involving several fatty acyl-CoA dehydrogenases having varied chain length specificities (Schulz, 1991, and references therein). Among them, the medium-chain fatty acyl-CoA dehydrogenase (MCAD),[1] often referred to as general fatty acyl-CoA dehydrogenase, is the most prominent form of the enzyme found in the mammalian kidney cortex (Thorpe et al., 1979). Although this enzyme exhibits a preferential selectivity for medium fatty acid chain substrates (optimum being for C_8), it utilizes a broad range of substrates (albeit with lower efficiency) ranging from palmitoyl–CoA to butyryl–CoA (Crane et al., 1956; Thorpe et al., 1979). The fatty acyl–CoA dehydrogenase–catalyzed reaction (irrespective of the substrate specificity) is envisaged to proceed in two steps (Beinert, 1963). The first step is the abstraction of the proton and the hydride ion from the α and β carbons of the thioester respectively, yielding $FADH_2$ and enoyl-CoA (Ghisla et al., 1984; Frerman et al., 1980). The repetitive turnover of this reaction is maintained by oxidation of the reduced $FADH_2$ by transfer of electrons to suitable electron acceptors in the second step (Lehman & Thorpe, 1990). Under physiological conditions, the immediate electron acceptor is FAD bound to electron-transferring flavoproteins (ETF) (Crane & Beinert, 1956).

$$E\text{–}FAD + \text{fatty acyl-CoA} \rightleftharpoons E\text{–}FADH_2\text{–enoyl-CoA} \quad (1a)$$

$$E\text{–}FADH_2\text{–enoyl-CoA} + \text{acceptor}_{ox} \rightleftharpoons E\text{–}FAD\text{–enoyl-CoA} + \text{acceptor}_{red} \quad (1b)$$

Due to interesting features associated with this enzyme, kinetic/mechanistic investigations have received considerable attention in recent years. Some such features include: (1) characteristic absorption signals of the oxidized flavin nucleotide which undergoes significant changes upon reduction by the substrate (Beinert, 1963); (2) measurement of the initial rates of the enzyme-catalyzed reaction by coupling with a number of "colored" electron acceptors (Lehman & Thorpe,

† Journal Article No. 2047 of the North Dakota Agricultural Experiment Station. Supported by the American Heart Association, Dakota Affiliate.

* To whom correspondence should be addressed.

[1] Abbreviations: MCAD, medium-chain acyl-CoA dehydrogenase; IPCoA, 3-indolepropionyl-coenzyme A; IACoA, *trans*-3-indoleacryloyl-coenzyme A; HPLC, high-performance liquid chromatography; FPLC, fast performance liquid chromatography; TBAP, tetrabutylammonium phosphate; DEAE, (diethylamino)ethyl; TMAE, (trimethylamino)ethyl; $FcPF_6$, ferricenium hexafluorophosphate; PMS, phenazine methosulfate; DCPIP, 2,6-dichlorophenol-indophenol; FAD, flavin adenine dinucleotide; EDTA, ethylenediaminetetraacetic acid; Tris-HCl, tris(hydroxymethyl)-aminomethane hydrochloride; ETF, electron transferring flavoprotein.

0006-2960/92/0431-10564$03.00/0

1990); and (3) confinement of the reductive half-reaction to a single turnover (in the absence of electron acceptors) (Ghisla & Massey, 1989) due to the thermodynamic stability of the E–$FADH_2$–enoyl-CoA product (Steyn-Parve & Beinert, 1958). By utilizing butyryl/crotonyl-CoA as a substrate/product pair, Schopfer et al. (1988) have recently performed detailed kinetic studies of the MCAD-catalyzed reaction. These authors, besides validating their previous findings, have pointed out that the kinetic complexity of this enzyme is intrinsic to the formation of several nonproductive complexes (such as oxidized enzyme–crotonyl-CoA, reduced enzyme–butyryl-CoA, etc.) during the catalytic pathway. However, in all these previous studies, very little attempt has been made to understand the role of the enzyme site environment in modulating the substrate structure, and/or vice-versa, during MCAD catalysis. Our interest on this enzyme arose basically from the point of view of the role of protein structure in catalysis.

Toward this end, we deliberated that the structural–functional relationships of this enzyme could best be elucidated by utilizing a chromophoric substrate analogue. Since MCAD is known to tolerate aromatic group substitution at the omega end of the fatty acyl-CoA substrate (Knoop, 1904; McFarland et al., 1982), we decided to synthesize indolepropionyl-CoA (IPCoA) and indoleacryloyl-CoA (IACoA) as a substrate and product for the MCAD-catalyzed reaction, respectively. The synthesis of indolepropionyl-CoA as a potential substrate for MCAD was prompted both by the expected absorbance in the near visible region (Bernhard et al., 1965), as well as by the thermodynamic stability of its resultant product (indoleacryloyl-CoA) due to the extended conjugation of the α–β unsaturated center of the acryloyl-CoA moiety to the indole ring. Thus, the IACoA product would resist the intrinsic hydratase activity of the enzyme (Lau et al., 1986). As will be shown in the subsequent section, by utilizing IPCoA and IACoA as a chromophoric substrate/product pair, we have unraveled several mechanistic properties of this enzyme which would have not been discerned by utilizing aliphatic chain CoA substrates.

MATERIALS AND METHODS

Materials. Coenzyme A (sodium salt), acetoacetyl-CoA (sodium salt), and the free acid of octanoyl-CoA were purchased from Sigma. 3-Indolepropionic acid and *trans*-3-indoleacrylic acid were purchased from Aldrich. The (trimethylamino)ethyl (TMAE) FPLC column was purchased from EM Separations (Gibbstown, NJ). DEAE-Sephacel and phenyl-Sepharose (6 fast flow, high substitution) were purchased from Pharmacia. Tetrabutylammonium phosphate ion complexing agent was purchased from Chrom Tech, Inc. (Apple Valley, MN).

Methods. Most of the experiments described in this manuscript were performed at 25 °C in 50 mM potassium phosphate buffer (pH 7.6) containing 0.3 mM EDTA. Experiments involving pH effects were performed in the following buffers: For pH ranges between 6 and 8.0, 50 mM potassium phosphate buffer containing 0.3 mM EDTA was used; for pH ranges between 8.0 and 9.5, 0.1 M Tris-HCl plus 50 mM potassium phosphate buffer containing 0.3 mM EDTA was used.

Steady-state kinetic and spectral analyses were performed on a Perkin-Elmer Lambda 3B spectrophotometer. Transient kinetic investigations were performed on a Durrum stopped-flow spectrophotometer. Stopped-flow data collection and analysis were carried out as described by Srivastava et al. (1989). Other kinetic and ligand-binding analyses were performed by the nonlinear regression analysis program Enzfitter (Elsevier Biosoft).

MCAD was routinely assayed in the 50 mM potassium phosphate buffer (pH 7.6) containing 0.3 mM EDTA, utilizing 30 μM octanoyl-CoA and 200 μM ferricenium hexafluorophosphate ($FcPF_6$) as the electron acceptor as described by Lehman et al. (1990). MCAD concentrations were determined using an extinction coefficient of 15.4 mM^{-1} cm^{-1} at 446 nm (Thorpe et al., 1979).

Purification of MCAD. Enzyme purification was essentially carried out according to the procedure of Gorelick et al. (1982), with several modifications. These include (1) instead of DEAE-cellulose, we used DEAE-Sephacel for the both batch and column chromatographic procedures; (2) the calcium phosphate gel–cellulose column was replaced with an FPLC–TMAE column (1 × 15 cm). The enzyme, after ammonium sulfate precipitation and dialysis, was loaded onto the FPLC–TMAE column, which was previously equilibrated with 20 mM potassium phosphate buffer (pH 7.6). The enzyme was adsorbed on this column and was subsequently eluted using a 0–0.2 M NaCl gradient. The peak fractions containing enzyme activity were pooled. The ratio of A_{280}/A_{450} at this stage was approximately 9.0. (3) The matrix gel Blue A column was replaced by a FPLC phenyl-Sepharose column (6 fast flow; high substitution). The pooled protein fraction from the TMAE column was brought to 35% saturation of ammonium sulfate and was loaded on a phenyl-Sepharose FPLC column (1 × 15 cm), previously equilibrated with 20 mM potassium phosphate buffer (pH 7.6) containing 0.3 mM EDTA and 35% ammonium sulfate. The bound enzyme was eluted using a 35% saturation to 10% saturation decreasing ammonium sulfate gradient. The peak fractions containing enzyme activity had an A_{280}/A_{450} ratio of 5.4. The enzyme had a specific activity of 36 units/mg (1400 min^{-1}) using octanoyl-CoA and $FcPF_6$ as substrate and electron acceptor, respectively, and migrated as a single band on SDS–PAGE. The enzyme was dialyzed against 50 mM potassium phosphate buffer (pH 7.6), concentrated, and stored frozen at –20 °C.

Electron transport flavoprotein (ETF) was purified as described previously (Gorelick et al., 1982).

Synthesis of IPCoA and IACoA. IPCoA was synthesized from 3-indolepropionic acid using the *N*-hydroxysuccinimide ester method as described by Al-Arif and Blecher (1969), except thioglycolic acid was not used in the reaction mixture. IACoA was synthesized from *trans*-3-indoleacrylic acid using the mixed anhydride procedure (Bernert & Sprecher, 1977) except benzene was replaced by tetrahydrofuran (THF) as the solvent in the preparation of the mixed anhydride. The activated acids (ester or anhydride) were dissolved in THF and added slowly to a solution of CoASH, in 0.1 M $NaHCO_3$ and THF (1:1 ratio), maintained under a nitrogen atmosphere. The pH was maintained between 7.5 and 8.5 by addition of solid $NaHCO_3$. The extent of reaction was monitored by measuring the SH content by the DTNB method (Ellman, 1959). After conversion of the respective ester to the CoA derivative, the solution was filtered through a fiber glass filter, and the THF was removed by rotary evaporation at room temperature. The remaining aqueous phase was first filtered through a fiber glass filter, followed by filtration through a 0.2 μm millipore filter before purification on the C_{18} HPLC column.

The impure CoA derivative was loaded onto a semipreparative reverse-phase C_{18} column (Alltech) equilibrated with

10 mM tetrabutylammonium phosphate (TBAP) in water (solvent A). The CoA derivatives were bound to the column at this stage. The column was then washed with 40% solvent B (10 mM TBAP in 80% methanol) to remove some of the impurities. The CoA derivatives were eluted using a 40–80% solvent B gradient developed over 40 min at a flow rate of 1.8 mL/min. IPCoA fractions were identified by their conversion to IACoA in an MCAD-catalyzed reaction. IACoA fractions were identified by recording the absorption spectrum of the yellow fractions. The fractions containing the CoA derivatives were pooled, and the methanol was removed by rotary evaporation at room temperature. The contaminant TBAP was removed by rechromatography on the same C_{18} column in the absence of TBAP.

Determination of the Extinction Coefficients of IPCoA and IACoA. The extinction coefficients of IPCoA and IACoA were determined by measuring the amounts of thiol released upon hydrolysis of the CoA esters by hydroxylaminolysis (1 M NH_2OH, pH 7.0, 30 min, 37 °C) followed by estimation of the liberated thiol by the DTNB method (Ellman, 1959). The amount of thiol released were then correlated with the absorption of IPCoA and IACoA at 259 and 367 nm, respectively. The ϵ for IPCoA and IACoA by this procedure were found to be 18.2 mM^{-1} cm^{-1} (at 259 nm) and 26.5 mM^{-1} cm^{-1} (at 367 nm), respectively.

Steady-State Kinetic Experiments. The initial rates of the MCAD-catalyzed reaction at varying concentrations of IPCoA were measured at 367 nm in the presence of various electron acceptors, such as $FcPF_6$ (Lehman et al., 1990), PMS/DCPIP (Thorpe, 1981), ETF/DCPIP (Gorelick et al., 1982), or buffer-dissolved O_2. Most of the steady-state reactions were performed in a 1-mL volume (1-cm path length cell), except for the oxygen-dependent (oxidase) reactions, which were performed in a total volume of 13.0 mL (5-cm path length cell) containing 31 nM MCAD. The steady-state enzyme-catalyzed oxidase reaction was monitored (in the absence of any externally added electron acceptor) by following the absorbance changes at 367 nm due to conversion of IPCoA to IACoA.

Dissociation Constant of the MCAD–IACoA Complex. This parameter was determined by following the signal for interaction between MCAD and IACoA at 417 nm. A limiting amount of MCAD (0.7 μM) was titrated with increasing concentrations of IACoA in a 10-cm path length cuvette (initial volume, 25.0 mL), and the absorbance at 417 nm was recorded after each addition of IACoA. The absorbances of IACoA and MCAD were subtracted from the absorbance of the mixture after dilution correction. The free IACoA concentration was calculated from the fractional saturation of the enzyme–IACoA complex as described previously (Johnson & Srivastava, 1991).

Anaerobic Experiments. Buffers were degassed and bubbled with prepurified grade argon in alternate cycles. To ensure an absolutely anaerobic environment for absorption spectroscopic measurements, 1 mM glucose and 11 units/mL glucose oxidase were added to the sample and reference cuvettes.

Transient Kinetic Experiments. For MCAD–FAD and IACoA equilibration experiments, an equal volume (approximately 0.25 mL) of enzyme and IACoA (present in the appropriate buffer) were mixed in the stopped flow syringes at 0 time. The time-dependent changes in absorption either at 355 nm or at 417 nm were recorded with the help of the software mentioned above. For IACoA-concentration dependent relaxation studies, a fixed concentration of enzyme (0.8 μM) was mixed with increasing concentrations of IACoA ($[E]_{tot} < [IACoA]_{tot}$) in the stopped-flow syringes, and the increase in absorption at 417 nm was recorded. The displacement of IACoA from the enzyme site was monitored at 417 nm by mixing 8 μM enzyme + 14 μM IACoA (syringe A) with 400 μM acetoacetyl-CoA (syringe B).

pH Jump Experiments. These experiments were performed by mixing a solution of MCAD/IACoA, maintained at one pH, with a concentrated buffer at the other pH in the stopped flow syringes and recording the absorption changes at 417 nm as described above. For a low to high pH jump, syringe A contained 4 mM MCAD and 80 mM IACoA in 10 mM monobasic potassium phosphate (pH 6.4), and syringe B contained 40 mM potassium phosphate (pH 10.4). Upon mixing, the pH of the solution changed to pH 9.0. For a high to low pH jump experiment, syringe A contained 4 μM MCAD and 80 μM IACoA in 10 mM potassium phosphate pH 9.0, and syringe B contained 40 mM monobasic potassium phosphate. Upon mixing, the pH of the mixture changed to 6.42.

Table I: Steady-State Kinetic Parameters for IPCoA in the MCAD-Catalyzed Reaction[a]

electron acceptor	apparent K_m ($M \times 10^{-6}$)	apparent K_{cat} (s^{-1})	K_{cat}/K_m (M^{-1} s^{-1})
$FcPF_6$	10.3 ± 0.6	0.46 ± 0.01	44 700
PMS/DCPIP	14.6 ± 1.7	0.28 ± 0.01	19 200
ETF/DCPIP	6.3 ± 0.4	0.25 ± 0.01	39 700
O_2	0.49 ± 0.04	0.016 ± 0.0004	32 600

[a] The concentration of MCAD was 92 nM in the PMS/DCPIP (PMS = 1.4 mM, DCPIP = 30 μM) and ETF/DCPIP (0.68 μM ETF, DCPIP = 30 μM) acceptor mediated enzyme-catalyzed reactions. Reactions involving $FcPF_6$ as the electron acceptor (200 μM) contained 60 nM MCAD. Oxidase reactions (240 μM oxygen) contained 31 nM enzyme.

RESULTS

Following the synthesis and purification of 3-indolepropionyl-CoA (IPCoA) and *trans*-3-indoleacryloyl-CoA (IACoA) (see Materials and Methods), we examined their UV–vis spectral properties in 50 mM phosphate buffer, pH 7.6 (data not shown). Of these CoA derivatives, IACoA is specifically characterized by its absorption maximum at 367 nm, due to the extended conjugation of the α–β double bond of the acrylic thioester moiety to the aromatic indole ring. The molar absorption coefficient of IACoA at 367 was determined to be 26 500 ± 400 M^{-1} cm^{-1} (see Materials and Methods).

We tested the effectiveness of IPCoA as a substrate for the MCAD-catalyzed reaction in the presence of several electron acceptors (Table I). For electron acceptors employed in this study, the apparent K_m (for IPCoA) and k_{cat} values (k_{cat}/K_m = 40 000 M^{-1} s^{-1}) practically remain invariant with changes in the chemical structure of the electron acceptors. However, IPCoA is about 500-fold less efficient than octanoyl-CoA as judged by the ratio of k_{cat} to K_m utilizing $FcPF_6$ as an electron acceptor (Lehman et al., 1990). Unlike octanoyl-CoA, the repetitive turnover of the MCAD-catalyzed conversion of IPCoA to IACoA is maintained by the electron acceptor role of the buffer-dissolved molecular oxygen. Such an "oxidase" activity of this enzyme has been reported for a number of other substrates including furylpropionyl-CoA (McFarland et al., 1982; Wang & Thorpe, 1991). Like other electron acceptor-dependent dehydrogenation reactions, the oxidase reaction also exhibits a Michaelian dependence on the IPCoA concentration with apparent K_m and k_{cat} values (for a buffer-dissolved oxygen concentration of 240 μM) of 0.49 ± 0.04

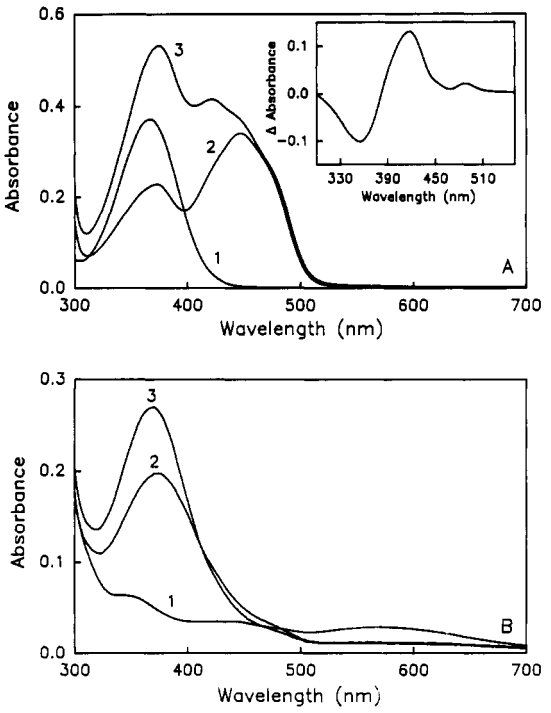

FIGURE 1: (A) UV–vis absorption spectra of IACoA, MCAD–FAD, and MCAD–FAD–IACoA in the standard phosphate buffer (pH 7.6). [IACoA] = 14 μM (1), [MCAD–FAD] = 22 μM (2), and the mixture of 14 μM IACoA and 22 μM MCAD-FAD (3). The inset shows the difference spectrum which was generated by subtracting the individual spectra of both MCAD–FAD and IACoA from their mixture. (B) UV–vis is absorption spectra of MCAD–$FADH_2$. These spectra were generated by incubating MCAD–FAD (10 μM) either with 16 μM IPCoA (curve 2) or with 32 μM IPCoA (curve 3) under anaerobic conditions. Curve 1 shows the analogous spectrum generated by incubating MCAD–FAD (10 μM) with 24 μM octanoyl CoA.

μM and 0.016 ± 0.0004 s^{-1}, respectively (Table I). Note that both these parameters are at least an order of magnitude lower than that observed for the dehydrogenation reaction (Table I).

UV–Visible Spectral Properties of the MCAD–IACoA Complex. Due to the chromophoric nature of IACoA, we were able to examine the influence of the enzyme site environment on its electronic structure. Figure 1 shows the UV–visible absorption spectra of IACoA, MCAD–FAD, and the mixture of IACoA and MCAD–FAD (MCAD–FAD > IACoA > K_d for the MCAD–FAD–IACoA complex). Note that the spectral features of both IACoA and FAD are perturbed in the complex. Of the two flavin peaks (one at 450 nm and the other at 370 nm), the higher wavelength peak (450 nm) is blue-shifted with marked hyperchromicity and emergence of two shoulders at 425 and 490 nm. Unlike the obvious spectral perturbations in the 450-nm region, the 370-nm peak of the flavin is considerably masked by the high absorption of IACoA (λ_{max} = 367 nm), and thus its spectral feature is not as explicit. Similarly, due to a finite contribution of the flavin absorption in the 367-nm region, the spectral perturbation of IACoA at the enzyme site phase is not clearly discernable. However, as a result of the higher ε of IACoA (at 367 nm) than that of the lower wavelength (370-nm) peak of the oxidized flavin, the absorption spectrum of the mixture of MCAD–FAD and IACoA (around 370 nm) is predominantly contributed by the IACoA absorption. Hence, we attribute that the 375-nm absorption peak of the mixture (Figure 1A) is the red-shifted absorption peak of the enzyme-bound IACoA. A further confirmation of the red-shifted absorption peak of IACoA comes when the latter is bound to the $FADH_2$ form of the enzyme (Figure 1B). In Figure 1B, we have compared the absorption spectra of octanoyl-CoA and IPCoA-reduced MCAD–FAD. Note that the flavin absorption peaks at both the 450- and 370-nm regions are substantially diminished when MCAD–FAD is reduced by octanoyl-CoA. Thus, the contribution of the 370-nm absorption peak of the flavin is minimal in the MCAD–$FADH_2$–IACoA complex. Therefore, the observed absorption peak at 373 nm must be the red-shifted peak of IACoA. It is noteworthy at this point that the magnitude of the red-shift of IACoA (bound to MCAD–$FADH_2$) is a function of the total IPCoA concentration (utilized to reduce MCAD–FAD to MCAD–$FADH_2$); high concentrations of IPCoA competitive displace MCAD–$FADH_2$-bound IACoA into the aqueous solution (curve 3, Figure 1B), and thus the resultant spectrum is a mixture of the free as well as enzyme-bound IACoA. These, as well as the other supporting evidence (see Discussion), lead us to propose that the absorption peak of IACoA is indeed red-shifted within the enzyme site phase. Furthermore, this red-shift in the IACoA spectrum is an exclusive property of the enzyme site phase, since attempts to simulate qualitatively similar spectral features either by changing the pH or polarity of the media were unsuccessful (data not shown).

Figure 1A (inset) shows the resultant spectrum of the MCAD–IACoA complex. This spectrum is generated by subtracting the contributions of individual chromophoric species (i.e., FAD and IACoA) from the mixture. Note that there are two major peaks at 417 (positive) and 355 (negative) and a minor peak at 490 nm (positive). By utilizing the 417-nm absorption signal, we have determined the dissociation constant for the MCAD–FAD–IACoA complex by titrating a limiting concentration of enzyme by an increasing concentration of IACoA. From the best fit of the experimental data, we have ascertained the dissociation constant of the enzyme–IACoA complex to be 2.7 ± 0.35 μM at pH 7.6 (data not shown). By following the same titration protocol, we determined the dissociation constant for the enzyme–IACoA complex at several pH values between pH 6.0 and 8.0 (data not shown). However, due to weak spectroscopic signals for the E*–IACoA complex at pH values higher than 8.0, we could not measure the dissociation constant for the E–IACoA complex at pH's around 9.0–9.5. To obtain this parameter, we performed a steady-state kinetic experiment for the conversion of IPCoA to IACoA in the absence and presence of IACoA at pH 9.5 and found the K_i to be equal to 30.3 ± 3.25 μM (data not shown). This value was taken to be a measure of the dissociation constant of the E–IACoA complex at pH 9.5.

We have examined the effect of pH on the resultant spectra of the MCAD–FAD–IACoA complex (Figure 2). Note that the maximum difference in absorbance is obtained at lower pH values; at pH 6.0, the absorbance maxima is found at wavelengths of 420 and 490 nm with a minimum at 355 nm. As the pH increases, the intensities of these absorption peaks decrease and undergo slight blue-shifts. Furthermore, these pH-dependent spectra show two isosbestic points at 295 and 390 nm, suggesting a pH-dependent distribution between two (protonated and nonprotonated) forms of the E–IACoA complexes.

To ensure that the pH-dependent spectral changes (shown in Figure 2) are not a result of impaired binding of IACoA with MCAD–FAD, we initially attempted to measure these spectra at saturating concentrations of the chromophoric species. However, due to the strong absorption of the individual chromophores, when utilized at high concentrations, the pH-

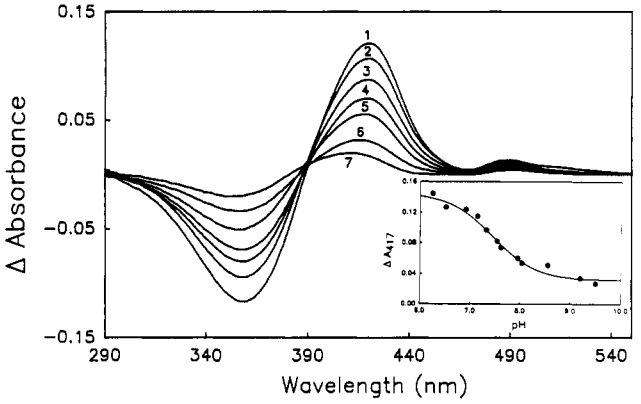

FIGURE 2: pH-dependent UV–vis spectra of the MCAD–IACoA complex. These spectra have been generated by subtracting the contribution of the individual chromophoric species (i.e., MCAD and IACoA) from their mixture. [MCAD] = 10 μM; [IACoA] = 8 μM. The pH values of the incubation mixture for these spectra are (1) 6.2, (2) 6.6, (3) 6.9, (4) 7.2, (5) 7.6, (6) 8.0, and (7) 8.9. The inset shows the dependence of absorbance at 417 nm as a function of pH. The solid line is the best fit of the experimental data according to the Henderson–Hasselbalch equation for a single proton equilibration process having a pK_a of 7.45. A saturating concentration of IACoA (80 μM) was used for all the pH values. [MCAD] = 8 μM.

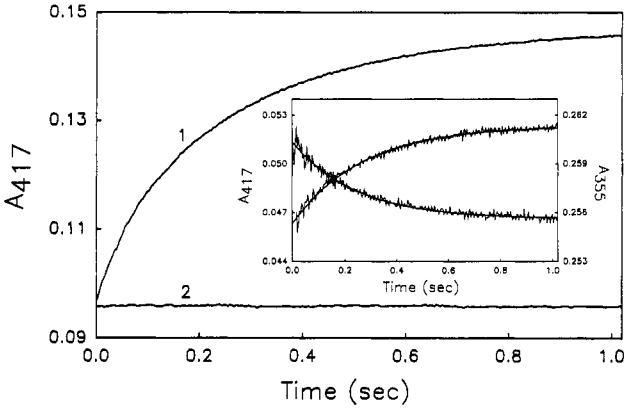

FIGURE 3: Representative stopped flow traces for the interaction of MCAD with IACoA at pH 6.4. Trace 1 indicates the change in absorbance at 417 (A_{417}) with time upon mixing 6.6 μM MCAD (syringe A) with 40 μM IACoA (syringe B) in the stopped-flow syringes at zero time. Trace 2 is simulated by adding the absorption changes of both IACoA and MCAD at 417 nm when they were mixed against buffer under similar conditions. Inset: Representative stopped flow traces for the changes in absorbance at 417 and 355 nm with respect to time for the interaction of MCAD with IACoA under pseudo-first-order conditions. Syringe A = 0.8 μM MCAD; syringe B = 20 μM IACoA. Increasing and decreasing traces represent the absorption changes at 417 and 355 nm, respectively. Solid lines are the best fit of the experimental data by the first-order rate equation. The rate constants for this reaction are 3.75 and 4.12 s^{-1} at 417 and 355 nm, respectively.

dependent difference spectra were not clearly resolved, particularly at the lower wavelength region (data not shown). Recourse was made to the direct measurement of pH-dependent differences in absorbance changes at 417 nm (the wavelength maxima of the difference spectra) upon incubation of 8 μM MCAD–FAD and 80 μM IACoA (Figure 1, inset); these concentrations were judged (on the basis of the K_d or K_i for the E–IACoA complex) to provide a 90% saturation of MCAD–FAD by IACoA at all pH values except for the last two experimental points; at pH's 9.2 and 9.5 the percent saturation of MCAD–FAD by IACoA was 80% and 72%, respectively. The solid line (Figure 2, inset) represents the best fit of the experimental data according to the Henderson–Hasselbalch equation (for a one-proton equilibration process) with a pK_a of 7.45. Since we could not perform pH-dependent spectral titration studies below pH 6.0 due to technical problems, it is difficult to quantitate the number of the proton equilibration steps (i.e., whether more than one protonation step is responsible for these changes). Furthermore, since the pH-dependent spectral changes observed during these static titration experiments are the result of a complex mixture of several coupled equilibria (rather than to a single protonation/deprotonation step, as observed for the dependence of k_2 and k_{-2} in Figure 5), we prefer to limit our discussion based on these findings. The only information utilized from these findings (to discuss the overall model presented in Scheme I) is the fact that the resultant spectra of the MCAD–FAD–IACoA complex undergo pH-dependent changes with a common isosbestic point, and thus they originate as a result of equilibration between protonated and nonprotonated forms of the enzyme–IACoA complex (see Scheme I).

Transient Kinetic Studies for the Interaction of Enzyme with IACoA. Having discerned the two pH-dependent forms of the E–IACoA complex, and that these forms are spectroscopically distinct, we proceeded to investigate the microscopic path(s) of their formation starting from the free enzyme and IACoA. When enzyme and IACoA were mixed ([IACoA] $\gg$ [E]) in the stopped-flow syringes at 0 time, the time-dependent increase in absorption at 417 nm, or decrease in absorption at 355 nm, could be easily monitored (Figure 3, inset). These time-dependent traces are consistent with single exponential processes with rate constants of 3.75 and 4.12 s^{-1} at 417 and 355 nm, respectively. To account as to whether any absorbance changes took place within the dead time of our stopped flow (5 ms), we recorded the absorbance of both the enzyme and IACoA when individually mixed against buffer. As shown in Figure 3, the sum of the individual absorbance of the enzyme and IACoA (at 417 nm) at all time regions is equal to the absorbance (at 417 nm) detected at 0 time when enzyme and IACoA were mixed in the stopped flow syringes. This observation attests to the fact that practically no detectable absorbance changes took place (at 417 nm) within the dead time of our stopped flow when enzyme and IACoA were mixed together, and most of the absorbance changes occurred during the observed relaxation time (see Discussion).

To ascertain whether the observed relaxation process is a result of a single-step enzyme/IACoA equilibration reaction or not, we measured the IACoA concentration-dependent (under conditions of [E] $\ll$ [IACoA]) relaxation rate constants (k_{obs}). As shown in Figure 4, the k_{obs} shows a hyperbolic dependence on the IACoA concentration. This precludes the possibility of a single-step equilibation reaction between enzyme and IACoA (see Discussion). Qualitatively similar results have been obtained for the interaction of MCAD–FAD with acetoacetyl-CoA (unpublished results).

From the IACoA concentration-dependent k_{obs} (at pH 6.4) of Figure 4, we have been able to calculate the limiting relaxation rate constant at zero, and saturating concentrations of IACoA, as well as the concentration of IACoA required to achieve half of the k_{obs} between extrapolated zero and infinite concentrations of IACoA. As will be elaborated under Discussion, for fast equilibrium conditions, these parameters, respectively, represent k_{-2a}, ($k_{2a} + k_{-2a}$), and K_{ca} for the acidic form of the enzyme (see Scheme I). While calculating these parameters, we realized that the maximum uncertainty lies in the determination of k_{-2a}, since its magnitude depends upon the extrapolation of the hyperbolic curve to zero concentration of IACoA. Furthermore, when we attempted to determine k_{obs} as a function of the IACoA concentration at pH's higher

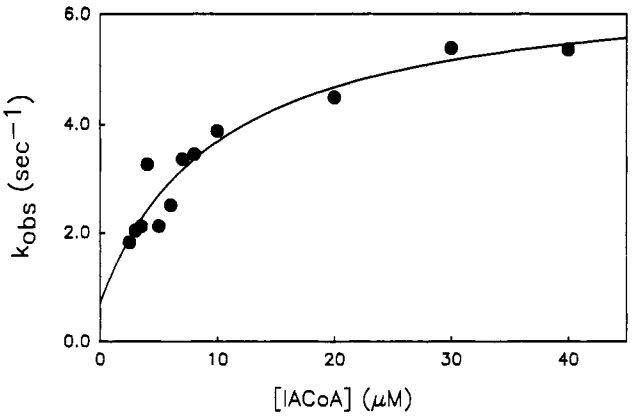

FIGURE 4: IACoA-concentration-dependent relaxation rate constant (k_{obs}) for the interaction of MCAD with IACoA measured at 417 nm. The experimental conditions are similar to those of Figure 3. After mixing, the concentration of MCAD was 0.4 μM. The IACoA concentration on the x axis represents the concentration after mixing. The solid line represents the best fit of the data according to the Michaelis–Menton equation with offset. The maximum k_{obs}, half saturation, and y intercept are 6.65 s^{-1}, 9.9 mM, and 0.7 s^{-1}, respectively.

than 7.5, the hyperbolic dependence (such as shown in Figure 4) was not clearly obvious. This was because the difference in k_{obs} between zero and saturating conditions of IACoA narrowed down at higher pH values. These observations prompted us to design an alternate experimental method for the determination of the macroscopic rate constant k_{-2} (see Discussion) with precision at all pH values. In this pursuit, we observed that acetoacetyl-CoA competitively displaces enzyme-bound IACoA, and such displacement results in a loss of the characteristic spectral properties of the enzyme–IACoA complex (data not shown). We comprehended that the displacement of IACoA from the enzyme site by an excessive concentration of acetoacetyl-CoA might provide a measure of k_{-2} (eq 2). In order for this approach to be

$$\text{E}^*\text{–IACoA} \rightleftharpoons \text{E–IACoA} \rightleftharpoons \text{E} + \text{IACoA}$$
$$\text{E–IACoA} + \text{AcAcCoA} \rightarrow \text{E–AcAcCoA} \qquad (2)$$

successful, two criteria were expected to be met: (1) the dissociation of E*–IACoA must follow the reverse path of E and IACoA association and (2) the rates of E–IACoA → E + IACoA and E + acetoacetyl-CoA → E–acetoacetyl-CoA must exceed E*–IACoA → E-IACoA conversion. The first criterion is naturally met according to the principle of microscopic reversibility. The second criterion was satisfied by experimental design involving high concentrations of acetoacetyl-CoA. Although formation of the E–acetoacetyl-CoA collision complex also undergoes an isomerization reaction to yield an E*–acetoacetyl-CoA complex (data not shown), the observed rate constant for this isomerization step is at least 10–15 times faster than that for the E–IACoA ⇌ E*–IACoA isomerization step. Hence, we could justify that the disappearance of the E*–IACoA complex in the presence of an excessive concentration of acetoacetyl-CoA must provide an accurate measure of k_{-2}.

Figure 5A (inset) shows the time-dependent disappearance of absorption at 417 nm upon mixing 400 μM acetoacetyl-CoA and a mixture containing 8 μM enzyme and 14 μM IACoA at pH 6.4 in the stopped-flow syringes. The experimental data are consistent with a single-exponential process, with a rate constant of 0.53 s^{-1}. This value is comparable to

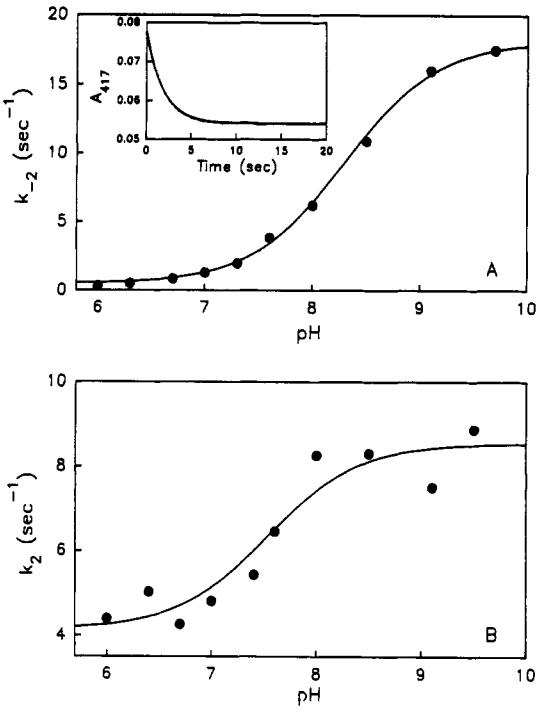

FIGURE 5: (A) Effect of pH on k_{-2}. Measured by the acetoacetyl-CoA displacement method, 8 mM MCAD + 14 μM IACoA (syringe A) was mixed with 400 μM acetoacetyl-CoA (syringe B). The solid line is the best fit of the experimental data according to the Henderson–Hasselbach equation with limiting maximum and minimum values for k_{-2} being 18.2 and 0.5 s^{-1}, respectively, and a pK_a equal to 8.3. The inset shows a representative stopped-flow trace for acetoacetyl-CoA displacement of IACoA from the MCAD site at pH 6.4. The solid line is the best fit of the experimental data according to the first-order rate equation with the rate constant equal to 0.53 s^{-1}. (B) Effect of pH on k_2. k_2 was calculated by subtracting k_{-2} from the relaxation rate constant ($k_2 + k_{-2}$) for the equilibration of MCAD with IACoA. Due to the difference in signal intensity as a function of pH, two sets of concentrations were used for relaxation rate constant measurements. Below pH 7.6, 1.6 μM MCAD (syringe A) was mixed with 50 μM IACoA (syringe B). At and above pH 7.6, 4.8 μM MCAD (syringe A) was mixed with 80 μM IACoA (syringe B). The solid line represents the best fit of the experimental data with limiting minimum and maximum values for k_2 being 8.1 and 4.23 s^{-1}, respectively, and a pK_a equal to 7.53.

k_{-2} at pH 6.4 (0.7 s^{-1}) obtained from the extrapolation of the k_{obs} versus IACoA plot to zero concentration of IACoA, as shown in Figure 4.

Effect of pH on k_2 and k_{-2}. Initially, we performed all the relaxation experiments at pH 6.4 because the signals for the E–IACoA interactions were maximum at lower pH values (see Figure 2). To observe the effect of pH on the macroscopic rate constants for the E–IACoA ⇌ E*–IACoA isomerization step, we measured the relaxation rate constants in the presence of saturating concentrations of IACoA (for measuring $k_2 + k_{-2}$) and used the acetoacetyl-CoA displacement method for measurement of k_{-2}. From these measurements, we could obtain the values of both k_2 and k_{-2} [$k_2 = (k_2 + k_{-2}) - k_{-2}$] at all pH values. Figure 5 shows the dependence of k_2 and k_{-2} on the pH of the buffer media. The solid lines are the best fit of the experimental data according to the Henderson–Hasselbalch equation; the pK_a's calculated from the data of k_2 and k_{-2} are 7.53 and 8.3, respectively. As will be elaborated under Discussion, the pK_a of 7.53 refers to the dissociability of the EH–IACoA collision complex, whereas the pK_a of 8.3 refers to the dissociability of the EH*–IACoA isomerized complex.

pH Jump Relaxation Studies. From the data of Figure 5, it is noteworthy that as the pH increases, both k_2 and k_{-2}

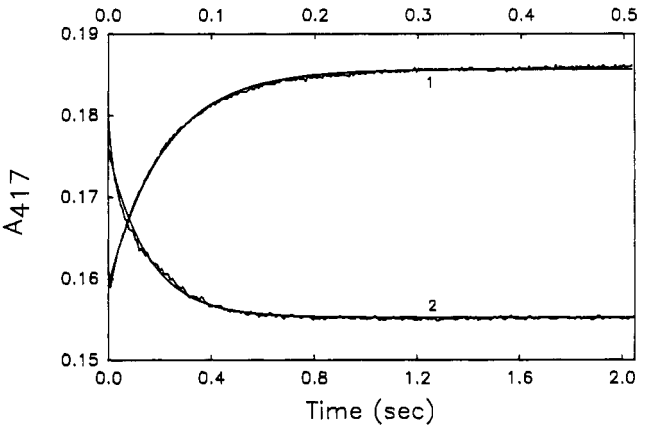

FIGURE 6: Time-dependent changes in absorption at 417 nm of the MCAD–IACoA complex upon pH jump. Trace 1 (bottom x axis), pH jump from 9.0 to 6.4; trace 2 (top x axis), pH jump from 6.4 to 9.0 (see Materials and Methods). The solid lines are the best fit of the experimental data according to the first-order rate equation with rate constants of 4.53 s^{-1} for trace 1 and 26.1 s^{-1} for trace 2.

increase, but the ratio of k_2/k_{-2} decreases. For example, at pH 6.4 this ratio is 9.86, whereas at pH 9.5 this ratio is only 0.43. Since at this pH extrema either protonated (at pH 6.4) or nonprotonated (at pH 9.5) forms of the free enzyme or enzyme–IACoA complexes predominate, it is apparent that the isomerization equilibrium is 20 times in favor of the E*–IACoA complex at lower pH than at higher pH (see Discussion). To further establish that the isomerization equilibria between E–IACoA $\rightleftharpoons$ E*–IACoA and EH–IACoA $\rightleftharpoons$ EH*–IACoA are linked via a proton association/dissociation step, we performed pH jump studies both from pH 6.4 to 9.0 as well as from pH 9.0 to 6.4. These studies were possible due to the difference in spectra between the acidic and basic forms of the enzyme–IACoA complexes and due to the fact that the magnitude of absorption at 417 nm due to the EH*–IACoA complex was approximately 5-fold higher than that due to the E*–IACoA complex (see Figure 2).

Figure 6 shows the changes in absorbance at 417 nm when the pH of the enzyme–IACoA mixture was changed from pH 9.0 to 6.4 (trace 1) or from 6.4 to 9.0 (trace 2). In either case the enzyme–IACoA mixture, maintained at a particular pH, was mixed with a high concentration of buffer of the other pH, such that the pH of the mixture was instantaneously altered (jumped). Note that the time-dependent changes in absorbance at 417 nm (relaxation traces), either from a low to high pH jump or vice versa, are best fitted by a first-order equation. It is further noteworthy that the amplitude of absorption changes either during the high to low pH jump or vice versa are remarkably similar. The observed (relaxation) rate constant obtained from the high to low pH jump experiment is 4.53 s^{-1} (curve 1, Figure 6). This value is remarkably similar to the relaxation rate constant observed for the isomerization of the EH-IACoA $\rightleftharpoons$ EH*–IACoA complex at pH 6.4 (6.65 s^{-1}). This attests to the fact that the proton equilibration steps (involving both collision as well as the isomerized enzyme–IACoA complexes) are faster than the isomerization step of the protonated form of the enzyme. Unlike these results, we did not anticipate a first-order relaxation rate (with a comparable magnitude) during the low to high pH jump experiment (curve 2, Figure 6). This is because proton equilibration reactions are assumed to be a rapid equilibrium process. However, under such conditions more than 70% of the color changes of the EH*–IACoA would have taken place within the dead time of the stopped flow (since the E–IACoA complex is favored over the E*–IACoA complex at high pH). This is contrary to our experimental observation; the magnitude of color changes observed either from the high to low pH jump or from the low to high pH jump experiment is the same. Interestingly, the relaxation rate constant obtained from the low to high pH jump experiment (26.1 s^{-1}) is once again similar to the relaxation rate constant for the E–IACoA $\rightleftharpoons$ E*–IACoA complex at pH 9.1 (23.5 s^{-1}, see Figure 5). Although we are unable to offer a clear explanation for this paradox, it is possible that its origin lies in the near equality in the relaxation rate constants of other steps (Bernasconi, 1976).

As mentioned earlier, due to weak spectroscopic signals of the E–IACoA complex at higher pH values, we failed to measure their dissociation constants. This, coupled with the near equality in rate constants for the E–IACoA $\rightleftharpoons$ E*–IACoA isomerization reaction at higher pH values, precluded us from experimentally measuring the value of K_c at the higher pH limit (i.e., K_{cb}). This forced us to adopt an indirect stratagem to quantitate the value of K_{cb}. Since the K_i for IACoA determined at pH 9.5 is equal to 30.3 ± 3.3 μM, (see above) and can be taken to be a measure of the K_d for enzyme–IACoA complex at pH 9.5, we could calculate K_c at pH 9.5 from the relationship K_d (K_i) = $K_c \times k_{-2}/k_2$. The K_c thus calculated (15.2 μM) for the basic form of the enzyme (at pH 9.5) was found to be of the same order as the K_c (9.9 μM) determined for the acidic form of the enzyme (at pH 6.4).

DISCUSSION

Characterization of MCAD Utilizing IPCoA/IACoA as Chromophoric Substrate Analogues. Medium-chain fatty acyl-CoA dehydrogenase represents a class of enzyme that tolerates considerable variability in its substrate structure (Knoop, 1904; Beinert, 1963; McFarland et al., 1982; Powell et al., 1987; Wang & Thorpe, 1991). This feature has allowed us to utilize 3-indolepropionyl/acryloyl-CoA (IPCoA/IACoA) as a chromophoric substrate/product pair to probe the catalytic pathway, as well as the microscopic environment of the enzyme active site. Due to the strong chromophoric nature of IACoA, it has been possible to measure the initial rates of the MCAD-catalyzed conversion of IPCoA to IACoA without recourse to spectral signals associated with externally added "colored" electron acceptors. Steady-state kinetic analysis for the MCAD-catalyzed reaction suggests that IPCoA serves as a competent substrate for the MCAD-catalyzed reaction. The ratios of k_{cat}/K_m for this enzyme involving IPCoA, butyryl-CoA, and octanoyl-CoA as substrates (under identical experimental conditions) are 2.4, 3.2, and 200 min^{-1} μM^{-1}, respectively. This suggests that, although IPCoA is not as efficient as octanoyl-CoA for this enzyme, it is comparable to butyryl-CoA, the substrate extensively utilized in mechanistic studies (Crane et al., 1956; Schopfer et al., 1988). Besides the dehydrogenation reaction, IPCoA has been found to undergo an enzyme-catalyzed oxidation reaction. Such oxidase reactions have been found for a number of other MCAD substrates (McFarland et al., 1982; Wang & Thorpe, 1991). The steady-state kinetic parameters for this oxidase reaction are, interestingly, found to be lower than that for the dehydrogenase reaction. We are currently investigating the detailed microscopic path of this oxidase reaction, and we will report our findings subsequently.

A major advantage in using IPCoA as the enzyme substrate, or IACoA as the chromophoric ligand, is the intrinsic thermodynamic stability of IACoA, particularly against the MCAD-catalyzed hydration reaction (Lau et al., 1986). Such

stability arises due to an extended conjugation of the π electrons of the "acryloyl" moiety of IACoA to the aromatic indole ring and is not expected with aliphatic chain CoA products. Consequently, the enzyme/product interaction could be probed more precisely with IACoA (without concern of contamination with its hydrated product), rather than with an aliphatic enoyl-CoA species. This, coupled with the fact that the absorption spectrum of IACoA exhibits characteristic spectral perturbations upon interaction with MCAD–FAD, has facilitated our investigation of the interaction of IACoA with the oxidized and the reduced forms of the enzyme.

Prior to this study, a number of investigators have performed spectral studies for the interaction of MCAD–FAD with aliphatic CoA substrate analogues (Auer & Frerman, 1980; Lau et al., 1988; Powell et al., 1987; Thorpe et al., 1981). In particular, Auer and Frerman (1980) have examined the influence of acetoacetyl-CoA, crotonoyl-CoA, octenoyl-CoA, octyl-CoA, and octanoyl-CoA on the absorption and CD spectral properties of the FAD and $FADH_2$ forms of the enzyme. However, due to the "transparent" (i.e., the absence of higher wavelength spectral bands) nature of these aliphatic CoA analogues, the only information available from these studies is the influence of the CoA analogues on the electronic structure (or asymmetry) of the flavin cofactor; no effect of the enzyme site environment on the electronic structures of these ligands is discernible. Such limitations do not apply, however, for IACoA as a chromophoric ligand. As noted under Results, the electronic spectra of both flavin and IACoA moieties are influenced upon binding of IACoA with MCAD–FAD. The 450-nm absorption band of MCAD–FAD is blue-shifted with marked hyperchromicity as well as with emergence of shoulders (due to resolution of vibrational structures) at 425 and 490 nm. These vibrational structures are more apparent on the CD spectra (data not shown), presumably due to the asymmetric nature of their transition dipoles (Johnson, 1985). It is interesting to note that, except for the appearance of an absorption band around 490 nm, both the absorption and CD spectra of the enzyme-bound FAD show different characteristic features in the presence of IACoA as compared with the other aliphatic CoA analogues. We attribute such differences to the aromatic nature of the indole ring of IACoA.

In contrast to the blue-shift in the FAD spectrum, the IACoA spectrum is red-shifted upon interaction with the oxidized as well as the reduced forms of the enzyme. The experimental evidence for such a red-shift in the IACoA spectrum (presented under Results) is further substantiated by following additional facts (our unpublished results): (1) Transient spectral analysis (via stopped flow, Princeton applied diode array rapid scan system) for the reductive half-reaction of MCAD–FAD with IPCoA reveals that the disappearance of the 450-nm oxidized flavin band is concomitant with the appearance of a transient spectral peak at 400 nm with a common isosbestic point at 426 nm. We attribute this 400-nm absorption peak to the red-shifted absorption peak of IACoA at the MCAD–$FADH_2$ site. The higher magnitude of the IACoA red-shift noted in the transient spectra, vis a vis the steady-state spectra (shown in Figure 1), is because during the transient phase all the IACoA (produced during reductive half-reaction) remains bound at the enzyme site and does not find sufficient time to exchange with the high concentration of IPCoA present in the reaction mixture. (2) We have recently observed that another chromophoric substrate analogue, β-furylacryloyl-CoA (initially utilized by McFarland and his collaborators) also gives a red-shift upon interaction with MCAD–FAD. The spectral red-shift of this furyl derivative is less interfered by the 370-nm flavin peak since it exhibits an absorption maximum at 335 nm (in contrast to the absorption maximum of IACoA at 367 nm). Qualitatively similar red-shifts in the absorption spectra of 4-thio-*trans*-2-octenoyl-CoA have been reported by Lau et al. (1989). All this evidence allows us to conclude that the absorption spectrum of IACoA is indeed red-shifted within the enzyme site phase.

A cursory examination of the enzymological literature dealing with the spectral perturbation of chromophoric substrates upon interaction with their cognate enzymes reveals that, although the blue-shift in chromophoric species can be attributed to the low polarity of the enzyme site phase, the red-shift is often caused by the extended conjugation of the π electrons of the chromophoric molecules in the ground state (Bernhard et al., 1965). Quite often the red-shift in chromophoric substrates has been shown to originate from the polarization of the adjacent carbonyl groups under the influence of some electrophilic groups of the enzyme site environment (Dunn & Hutchinson, 1973; Dunn et al., 1975), and such polarization results in the ground-state activation of the substrate structure (Belasco & Knowles, 1980, 1983). From these precedents, it is tempting to speculate that the carbonyl group of IACoA is polarized upon interaction with some electrophilic group of the MCAD site (eq 3). Since the

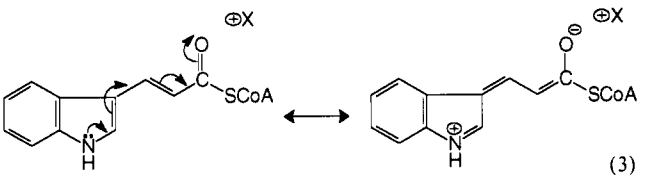

(3)

carbonyl polarization, as well as the attainment of the extended conjugation in the substrate structure, requires fine adjustments of the bond lengths and the bond angles, it is reasonable to expect complementary changes in the protein structure (at least in the vicinity of the substrate binding site) to stabilize the altered substrate structure. Thus, it is reasonable to assume that protein conformational changes are, in part, responsible for the observed electronic perturbations of the individual chromophoric species, although experimental evidence at the present time are not compelling.

In pursuit of investigating the molecular nature of the electrophilic group responsible for the polarization of the carbonyl group of IACoA, we realized that no metal ions are involved in either ligand binding or catalysis of MCAD (Beinert, 1963). This suggested that some basic amino acid residue of the active site must serve as an electrophile at its protonated state, and we were prompted to undertake the pH-dependent studies discussed in the following section.

pH-Dependent Changes in the Spectral, Kinetic, and Thermodynamic Properties of the MCAD–IACoA Complex. The pH-dependent studies allowed us to delineate the microscopic pathways by which the isomerization of the MCAD–IACoA complex is linked via the protonation/deprotonation step presented in Scheme I. However, before discussing the overall model (Scheme I) which conforms to the experimental data presented in the previous section, we would like to justify that the enzyme–IACoA relaxation studies satisfy a rapid equilibrium condition. This is important since many enzyme kineticists use (a priori) either a steady-state or a rapid equilibrium assumption to derive rate equations for two (or more)-step enzyme–substrate (ligand) equilibration reactions, despite the fact that these two assumptions require

entirely different relationships among the microscopic rate constants (Bernasoni, 1976; Johnson, 1991).

The fact that the observed relaxation rate constants for the interaction of enzyme with IACoA (measured under pseudo-first-order conditions) exhibit a hyperbolic dependence on the IACoA concentration suggests that the overall process proceeds in at least two sequential steps:

$$E + IACOA \underset{k_{-1}}{\overset{k_1}{\rightleftharpoons}} E\text{–}IACoA \underset{k_{-2}}{\overset{k_2}{\rightleftharpoons}} E^*\text{–}IACoA \quad (4)$$

Without making any assumptions (steady state or rapid equilibrium), the relaxation rate constants for this two-step process can be given by

$$\frac{1}{\tau_1} = \frac{1}{2}\{(k_1[IACoA] + k_{-1} + k_2 + k_{-2}) + [(k_1[IACoA] + k_{-1} + k_2 + k_{-2})^2 - 4(k_{-1}k_{-2} + k_1[IACoA]k_2 + k_1[IACoA]k_{-2})]^{1/2}\} \quad (5)$$

$$\frac{1}{\tau_2} = \frac{1}{2}\{(k_1[IACoA] + k_{-1} + k_2 + k_{-2}) - [(k_1[IACoA] + k_{-1} + k_2 + k_{-2})^2 - 4(k_{-1}k_{-2} + k_1[IACoA]k_2 + k_1[IACoA]k_{-2})]^{1/2}\} \quad (6)$$

These equations can be simplified by a square root approximation [i.e., $(1 - X)^{1/2} = 1 - 0.5X$, if $X \ll 1$] to yield

$$\frac{1}{\tau_1} = k_1[IACoA] + k_{-1} + k_2 + k_{-2} \quad (7)$$

$$\frac{1}{\tau_2} = \frac{k_1[IACoA](k_{-2} + k_2) + k_{-1}k_{-2}}{k_1[IACoA] + k_{-1} + k_2 + k_{-2}} \quad (8)$$

Equation 8 predicts a hyperbolic dependence of the observed rate constant as a function of the IACoA concentration, as was experimentally observed for the data of Figure 4. From the best fit of the experimental data of Figure 4 for a hyperbolic dependence, we have obtained the values for (a) the rate constant at zero concentration of IACoA [k_{obs} (min) = 0.7 s^{-1}], (b) the rate constant at infinite concentration of IACoA [k_{obs}(max) = 6.65 s^{-1}], and (c) the concentration of IACoA required to achieve half of the total variation in rate constants between zero and infinite concentration of IACoA (K_c = 9.9 μM). These values are a direct measure of the combined rate constants predicted by eq 8, viz., $k_{obs}(min) = k_{-1}k_{-2}/(k_{-1} + k_2 + k_{-2})$, $k_{obs}(max) = k_2 + k_{-2}$, and $K_c = (k_{-1} + k_2 + k_3)/k_1$. Although it is not possible to calculate all four rate constants from these three equations, the relative magnitudes of these rate constants can be obtained by arbitrarily selecting fixed values of k_1 and inserting this value in the above equations. At a saturating concentration of IACoA, k_{obs}(max) is always a measure of $k_2 + k_{-2}$. Given that the concentration of IACoA required to achieve half the relaxation rate constant between zero and infinite concentrations of IACoA is 9.9 mM (see Figure 4), a simple calculation reveals that, for [IACoA] = 9.9 μM and $k_1 > 10^7$ M^{-1} s^{-1}, the magnitudes of k_1 and k_{-1} are at least 20 times higher than those of k_2 and k_{-2}. This attests to the fact that the first step is in a rapid equilibrium. On the contrary, for similar conditions, if k_1 is 10^6 M^{-1} s^{-1} or smaller, the magnitudes of k_1 and k_{-1} are comparable to those of k_2 and k_{-2}, and thus does not satisfy the rapid equilibrium condition. Moreover, under such conditions (and for selected concentrations of IACoA), the observed relaxation profile would deviate from the single-exponential rate law (inconsistent with our experimental observations). The steady-state condition can only be satisfied under a limited set of these rate constants, with k_1 at least lower than 10^6 M^{-1} s^{-1}. From the precedents that the enzyme–substrate association is a diffusion-limited process, i.e., $k_1 = 10^8$ M^{-1} s^{-1} (Hammes, 1982), it is highly plausible that the first step of eq 4 is in rapid equilibrium. Unlike enzyme–substrate (ligand) equilibration reactions, the protonation/deprotonation reactions have unequivocally been accepted to proceed at much faster rates (Brocklehurst & Dixon, 1976, 1977), and thus these steps also satisfy rapid equilibrium conditions.

Scheme I

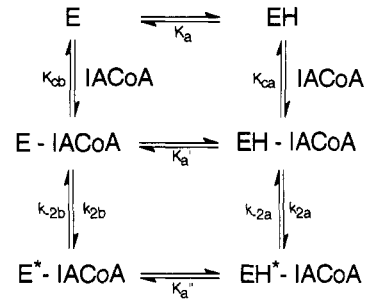

Having established that the enzyme–IACoA association, as well as the protonation/deprotonation reactions are rapid equilibrium steps, the experimental results presented in the previous section are consistent with a minimal model presented in Scheme I. According to this model, there are two distinct proton-dependent (acidic and basic) forms of the enzyme. These two forms independently combine with IACoA to form collision complexes (E–IACoA and EH–IACoA) which undergo slow isomerization reactions into more stable forms (E*–IACoA and EH*–IACoA). This slow isomerization step is concomitant with the spectral changes of the enzyme–IACoA complex, as evidenced by the increase in absorption at 417 nm. Since both E*–IACoA and EH*–IACoA contribute to the absorption at 417 nm (albeit to different magnitudes), their time-dependent appearance can be given by (see Appendix)

$$[E^*\text{–}IACoA] + [EH^*\text{–}IACoA] = \frac{\alpha[E_t]}{(\alpha + \beta)}[1 - e^{-(\alpha+\beta)t}] \quad (9)$$

where

$$\alpha = \frac{k_{2b}K_a'[IACoA] + k_{2a}[IACoA][H^+]}{K_{cb}K_a' + K_a'[IACoA] + K_{ca}[H^+] + [IACoA][H^+]} \quad (10)$$

$$\beta = \frac{k_{-2b}K_a'' + k_{-2a}[H^+]}{K_a'' + [H^+]} \quad (11)$$

E_t = total enzyme, and $(\alpha + \beta)$ is the observed relaxation rate constant (k_{obs}). At infinite concentrations of IACoA, eq 10 reduces to

$$\alpha = \frac{k_{2b}K_a' + k_{2a}[H^+]}{K_a' + [H^+]} \quad (12)$$

This equation is analogous to the dependence of β on pH (eq 11). At infinite concentrations of IACoA, α and β are a measure of the macroscopic forward (k_2) and reverse (k_{-2}) rate constants, respectively, for the slow isomerization reaction.

At limiting acidic and basic pH values, the corresponding microscopic rate constants are represented by the subscript

"a" (for acidic) and "b" (for basic) pH's. K_{ca} and K_{cb} are the dissociation constants for the EH–IACoA and E–IACoA collision complexes. K_a' and K_a'' are the proton dissociation constants for the EH–IACoA and EH*–IACoA complexes, respectively.

Consistent with the prediction of eq 9, all our enzyme/IACoA equilibration reactions (measured at 417 nm) conform to a single-exponential process, and both the amplitudes and the relaxation rate constants are functions of IACoA and proton concentrations. At limiting low pH values (i.e., at saturating proton concentrations), an equation for the apparent rate constant, k_{obs}, can be written as

$$k_{obs} = \frac{k_{2a}[\text{IACoA}]}{K_{ca} + [\text{IACoA}]} + k_{-2a} \quad (13)$$

From the experimental results of the hyperbolic dependence of the observed rate constant on the IACoA concentration at pH 6.4 (Figure 4), we could calculate the parameters (k_{2a}, k_{-2a}, and K_{ca}) (Table I). It is noteworthy that, under certain conditions, a sharp hyperbolic dependence of k_{obs} on ligand concentration (as observed in Figure 4) is not observed for the identical relaxation model (eq 4). These include the conditions (1) where the dissociation constant for the collision complex (K_c) is too small to maintain the concentration of E and IACoA under a pseudo-first-order condition ([E] $\ll$ [IACoA]) and monitor the absorbance changes or (2) where $k_2 < k_{-2}$ such that there is no measurable difference in the relaxation rate constant between the lowest and highest concentrations of IACoA. Our inability to discern the hyperbolic dependence at higher pH values was due to condition 2 (see Figure 5), and hence we were forced to rely on the acetoacetyl-CoA displacement method to determine k_{-2} (see Materials and Methods).

After assigning the microscopic parameters (k_{2a}, k_{-2a}, and K_{ca}) for the sequential steps of the EH–IACoA equilibration reaction at the lower pH range, it is possible to predict the dissociation constant for the EH*–IACoA complex. The predicted value can then be compared with the experimentally measured value under identical experimental conditions. However, such predictions require the precise assessment as to whether the intermediary collision complex EH–IACoA is a colored species (i.e., shows absorption at 417 nm) or not. On the basis that the formation of the EH–IACoA complex is controlled by a diffusion-limited process ($k_1 = 10^8\ M^{-1}\ s^{-1}$) and given the parameters calculated in the previous paragraph, we could predict that more than 63% of the total enzyme would predominate in the form of the EH–IACoA complex (within the 5 ms dead time of our stopped flow) under the experimental conditions of Figure 3. If the ϵ_{417} for the EH–IACoA complex were similar to that of the EH*–IACoA complex, approximately 63% of the total A_{417} would have occurred within the dead time of our instrument. In contrast to this expectation, practically no color changes were detected at 417 nm during this time (see Figure 3). Hence, we can conclude that the EH–IACoA collision complex is a colorless species and the observed color changes take place upon its isomerization to the EH*–IACoA complex:

$$\text{E} + \text{IACOA} \underset{k_{-1}}{\overset{k_1}{\rightleftharpoons}} \underset{\text{(colorless)}}{\text{E–IACoA}} \underset{k_{-2}}{\overset{k_2}{\rightleftharpoons}} \underset{\text{(colored)}}{\text{E*–IACoA}} \quad (14)$$

For this situation, the observed dissociation constant (K_d) measured by following the color changes at 417 nm upon titration of a limiting concentration of E at increasing concentrations of IACoA can be given by

$$K_d = \frac{[\text{E}][\text{IACoA}]}{[\text{E*–IACoA}]} = \frac{[\text{E}][\text{IACoA}]}{[\text{E–IACoA}]}\frac{[\text{E–IACoA}]}{[\text{E*–IACoA}]} = K_c\frac{k_{-2}}{k_2} \quad (15)$$

On the contrary, if both EH–IACoA and EH*–IACoA were colored species (with equal molar extinction coefficients), the observed K_d (by spectrophotometric titration experiments) would be given by $K_d = [\text{E}][\text{IACoA}]/([\text{EH–IACoA}] + [\text{EH*–IACoA}])$. In this situation, the relationship between the observed K_d and other microscopic parameters would be $K_d = K_c k_{-2}/(k_2 + k_{-2})$.

From the parameters obtained by the IACoA concentration-dependent relaxation studies (for a rapid equilibrium model), the calculated K_d for the E–IACoA complex (according to eq 15) is 1.16 μM. This value is remarkably similar to the experimentally observed K_d (1.07 μM) determined by following the color changes at 417 nm in a static experiment (data not shown).

The demonstration that no color changes take place upon initial formation of the enzyme–IACoA collision complex, whereas all the color changes take place upon isomerization of that complex, refines our conclusion drawn on the basis of "static" experiments involving the interaction of MCAD–FAD with IACoA (Figure 1). These new results emphasize that spectral changes arise as a result of slow isomerization of the enzyme–IACoA complex and that during this process the electronic structures of both the flavin and IACoA chromophores are altered. Although it is tempting to ascribe this slow isomerization reaction (responsible for the spectral changes) to the slow conformational changes in the MCAD protein structure, the experimental results presented herein are inadequate to rule out the following alternative possibilities: (1) Following the initial binding of IACoA with MCAD–FAD, both IACoA and FAD (slowly) readjust their positions within the enzyme site so that they are exposed to different polar environments. (2) The initial binding of IACoA follows a slow approach of individual chromophoric species in the vicinity of each other to the extent that their original electronic structures are perturbed. Among these two possibilities, the first, particularly for the polarity-dependent red-shift in the IACoA spectrum, can be easily discarded on the basis that such shifts have not been experimentally observed in the presence of solvents of different polarity (data not shown). Furthermore, the fact that the red-shift in the IACoA spectrum is observed upon interaction with either the FAD or $FADH_2$ form of the enzyme eliminates the possibility that the electron deficient ring of the flavin moiety in MCAD–FAD is responsible for the spectral shift of IACoA. However, we cannot rule out the possibility of polarity-dependent blue-shifts in the FAD spectrum. Unlike the environmental effect, the second possibility relies on the perturbation of the electronic structure of the individual chromophoric species via their close juxtaposition within the enzyme site phase. Since such a process can be envisaged to be sterically restricted, it is expected that the spectral changes must accompany the impaired binding of IACoA. This expectation is contrary to our experimental finding. It is noteworthy that the dissociation constant of the MCAD–FAD–IACoA collision complex (K_{ca} = 9.9 μM) is at least 9-fold higher than the dissociation constant (K_d = 1.07 μM) of the MCAD–FAD–IACoA

Table II: Kinetic/Thermodynamic Parameters for the Model of Scheme I

kinetic/thermodynamic parameter	value
k_{2b}	$8.10 \pm 0.64\ s^{-1}$
k_{-2b}	$18.2 \pm 0.32\ s^{-1}$
k_{2a}	$4.23 \pm 0.39\ s^{-1}$
k_{-2a}	$0.50 \pm 0.17\ s^{-1}$
K_{cb}	$15.2 \pm 1.12\ (\times 10^{-6}\ M)$
K_{ca}	$9.90 \pm 0.60\ (\times 10^{-6}\ M)$
$K_{a'}$	$4.53 \pm 2.54\ (\times 10^{-8}\ M)$
$K_{a''}$	$2.95 \pm 1.54\ (\times 10^{-8}\ M)$
K_a	$5.01 \pm 0.31\ (\times 10^{-9}\ M)$

isomerized complex. Clearly, the isomerization step has strengthened (rather than weakened) the binding affinity of IACoA for the enzyme site. Hence, the spectral changes during the isomerization step must involve complementary changes in the protein structure so that the resultant complex is thermodynamically stable; such coupled processes have been argued to be involved in enzyme-catalyzed reactions (Bernhard, 1982).

From the pH-dependent spectral changes (Figure 2), it is evident that the resultant absorption peaks increase in magnitude (without undergoing significant changes in their positions) as the pH of the media is decreased. This is suggestive that the electronic structures of both IACoA and FAD, in the E–IACoA complex, are equally influenced by changes in the pH of the buffer media and eliminates the possibility of an alternative mode(s) of IACoA binding with different (protonated versus nonprotonated) states of the enzyme. Since the spectral properties of both IACoA and MCAD–FAD remain practically unaffected with changes in the pH of the buffer media (data not shown), the binding of IACoA in alternate conformations with protonated and nonprotonated forms of the enzyme would be expected to yield different types of spectra (contrary to our experimental results). Thus, the pH-dependent spectral changes are consistent with the altered distribution between collision and isomerized complexes involving MCAD–FAD and IACoA (Scheme I, Table II).

The magnitude of this equilibrium distribution can be envisaged by examining the properties of eqs 10 and 11. At saturating concentrations of IACoA, eq 10 could be simplified to eq 12. Note that both eqs 11 and 12 are analogous to the modified form of the Henderson–Hasselbalch equation (Fersht, 1977), predicting a pH-dependent sigmoidal behavior of both k_2 and k_{-2}. Such predictions are verified from the experimental data of Figure 5. Thus, consistent with eq 11 and from the best fit of the pH versus k_{-2} plot (Figure 5A), we can calculate the values of k_{-2a}, k_{-2b}, and pK_a'' to be 0.5 s^{-1}, 18.2 s^{-1}, and 8.3, respectively. Similarly, as predicted by eq 12, from the data of pH versus k_2 (Figure 5B), we could calculate k_{2a}, k_{2b}, and pK_a' to be 4.23 s^{-1}, 8.1 s^{-1}, and 7.53, respectively. The corresponding dissociation constants for pK_a' and pK_a'' are 2.95×10^{-8} and 5.01×10^{-9} M, respectively. These values are summarized in Table II. Given that all the enzyme–IACoA ligated species are interconvertible (Scheme I) and that the free energy is a state function, the following relationship must be satisfied:

$$\frac{k_{2b}}{k_{-2b}}\frac{1}{K_a''} = \frac{1}{K_a'}\frac{k_{2a}}{k_{-2a}} \qquad (16)$$

Upon substituting the value for these constants (Table II), it is found that this relationship is off by only a factor of 3, which is within the limit of the experimental error in determining the individual microscopic parameters. With similar analogy, and given the values for K_{ca}, K_{cb}, and pK_a', we can calculate the K_a (4.53×10^{-8} M) for the proton dissociation step of the free enzyme; this K_a translates into a pK_a of 7.34.

A quick perusal of the pK_a's for the enzyme site group responsible for the color changes of the enzyme–IACoA complex reveals that the pK_a of the free enzyme is increased from 7.34 to 7.5 upon interaction with IACoA within the collision complex, whereas it is increased to 8.3 upon isomerization of the collision complex. Since the difference between pK_a of 7.34 and 7.5 is so small, its origin may lie in the uncertainty in determining the associated thermodynamic parameters (such as K_{ca}, K_{cb}, etc.). Alternatively, this difference may in fact be due to a decrease in the polarity of the media such that the proton dissociability of a neutral (uncharged) amino acid residue is impaired. Unlike such a small change in the pK_a during formation of the collision complex, a substantial increase in pK_a is noted within the isomerized complex. Since the isomerization of the collision complex is argued to accompany the changes in the protein conformation, it follows that the increase in pK_a from 7.5 to 8.3 is a result of the altered structure of the protein–IACoA complex.

From the data compiled in Table II, it is evident that K_{ca} and K_{cb} differ only by a factor 1.5. This means that the ligand binding equilibria are practically independent of the protonated state of the enzyme. In contrast, a significant (about 20-fold) change in equilibrium distribution between E–IACoA and E*–IACoA is observed between basic ($k_{2b}/k_{-2b} = 0.44$) and acidic ($k_{2a}/k_{-2a} = 8.46$) forms of the enzyme. Since this equilibrium step is a result of isomerization of the enzyme–IACoA complex (in which the conformation of both IACoA and enzyme are altered), it is clear that the isomerized complex is stabilized within the protonated state of the enzyme–IACoA complex, and this serves as the molecular basis for pH-dependent spectral changes.

The coupled equilibria involving E–IACoA isomerization and the proton equilibration reaction suggest that, at a neutral pH, the (basic) amino acid side chain group responsible for the color changes is only partially protonated both within the free enzyme site as well as in the enzyme–IACoA collision complex. However, as soon as the enzyme–IACoA complex is isomerized, a concomitant protonation of the amino acid side chain residue occurs (at the same neutral pH) thus increasing its pK_a value. In this way, the enzyme–IACoA isomerization step serves as an intrinsic pathway for providing an electrophilic enzyme site environment that is likely to be responsible for the polarization of the carbonyl group of IACoA.

APPENDIX

The total concentration of colorless [E_t] and colored [E^*_t] enzyme species (Scheme I) involved in ligation with IACoA (denoted by I) are represented by

$$[E_t] = [E] + [EI] + [EH] + [EHI]$$

$$[E^*_t] = [EI^*] + [EHI^*]$$

where E and EH are the unprotonated and protonated forms of the enzyme, respectively. The initial enzyme concentration, $[E]_0$, is thus represented by the sum of E_t and E^*_t

$$[E]_o = [E_t] + [E^*_t]$$

Since the enzyme species represented by E_t are in rapid

equilibrium, we can write expressions for each of the species:

$$[E] = \frac{K_{cb}K_a'[E_t]}{K_{cb}K_a' + K_a'[I] + K_{ca}[H] + [I][H]}$$

$$[EH] = \frac{K_{ca}[H][E_t]}{K_{cb}K_a' + K_a'[I] + K_{ca}[H] + [I][H]}$$

$$[EI] = \frac{K_a'[I][E_t]}{K_{cb}K_a' + K_a'[I] + K_{ca}'[H] + [I][H]}$$

$$[EHI] = \frac{[H][I][E_t]}{K_{cb}K_a' + K_a'[I] + K_{ca}'[H] + [I][H]}$$

Similarly, since E*I and E*HI are in rapid equilibrium we can write

$$[E^*I] = \frac{K_a''[E^*_t]}{K_a'' + [H]} \qquad [E^*HI] = \frac{[H][E^*_t]}{K_a'' + [H]}$$

The rate of appearance of colored enzyme–IACoA species (E^*_t) can be written as

$$\frac{d[E^*_t]}{dt} = k_{2b}[EI] + k_{2a}[EHI] - k_{-2b}[E^*I] - k_{-2a}[E^*HI]$$

Upon substituting the values for the enzyme species in parentheses, we obtain

$$\frac{d[E^*_t]}{dt} = \frac{k_{2b}K_a'[I] + k_{2a}[I][H]}{K_{cb}K_a' + K_a'[I] + K_{ca}[I] + [I][H]}[E_t] - \frac{k_{-2b}K_a'' + k_{-2a}[H]}{K_a'' + [H]}[E^*_t]$$

$$= \alpha[E_t] - \beta[E^*_t] = \alpha[E]_0 - (\alpha + \beta)[E^*_t]$$

where

$$\alpha = \frac{k_{2b}K_a'[I] + k_{2a}[I][H]}{K_{cb}K_a' + K_a'[I] + K_{ca}[H] + [I][H]}$$

$$\beta = \frac{k_{-2b}K_a'' + k_{-2a}[H]}{K_a'' + [H]}$$

If I is much greater than E (i.e., pseudo-first-order conditions), it can be regarded as a constant; and since H is constant, the rate equation can be integrated to yield

$$[E^*I] + [E^*HI] = \frac{\alpha[E_t]}{(\alpha + \beta)}[1 - e^{-(\alpha+\beta)t}]$$

which is the same as eq 9 under Discussion.

REFERENCES

Al-Arif, A., & Blecher, M. (1969) *J. Lipid Res. 10*, 344–345.
Auer, H. E., & Frerman, F. E. (1980) *J. Biol. Chem. 255*, 8157–8163.
Beinert, H. (1963) *Enzymes (2nd ed.) 7*, 447–466.
Belasco, J. G., & Knowles, J. R. (1980) *Biochemistry 19*, 472–477.
Belasco, J. G., & Knowles, J. R. (1983) *Biochemistry 22*, 122–129.
Bernasconi, C. F. (1976) *Relaxation Kinetics*, Academic Press, New York.
Bernert, J. T., & Sprecher, H. (1977) *J. Biol. Chem. 252*, 6737–6744.
Bernhard, S. A. (1982) *Stud. Org. Chem. (Amsterdam) 10*, 237–252.
Bernhard, S. A., Lau, S. J., & Noller, H. (1965) *Biochemistry 4*, 1108–1118.
Brocklehurst, K., & Dixon, H. B. F. (1976) *Biochem. J. 155*, 61–70.
Brocklehurst, K., & Dixon, H. B. F. (1977) *Biochem. J. 167*, 859–862.
Crane, F. L., & Beinert, B. (1956) *J. Biol. Chem. 219*, 717–731.
Crane, F. L., Mii, S., Hauge, J. G., Green, D. E., & Beinert, H. (1956) *J. Biol. Chem. 218*, 701–716.
Dunn, M. F., & Hutchinson, J. S. (1973) *Biochemistry 12*, 4882–4892.
Dunn, M. F., Biellmann, J., & Branlant, G. (1975) *Biochemistry 14*, 3176–3182.
Ellman, G. L. (1959) *Arch. Biochem. Biophys. 82*, 70–77.
Fersht, A. (1977) *Enzyme Structure and Function*, Freeman and Co., San Francisco.
Frerman, F. E., Miziorko, H. M., & Beckmann, J. D. (1980) *J. Biol. Chem. 255*, 11192–11198.
Ghisla, G., & Massey, V. (1989) *Eur. J. Biochem. 181*, 1–17.
Ghisla, G., Thorpe, C., & Massey, V. (1984) *Biochemistry 23*, 3154–3161.
Gorelick, R. J., Mizzer, J. P., & Thorpe, C. (1982) *Biochemistry 21*, 6936–6942.
Gorelick, R. J., Schopfer, L. M., Ballou, D. P., Massey, V., & Thorpe, C. (1985) *Biochemistry 24*, 6830–6839.
Hammes, G. G. (1982) *Enzyme Catalysis and Regulation*, Academic Press, New York.
Johnson, J. K., & Srivastava, D. K. (1991) *Arch. Biochem. Biophys. 287*, 250–256.
Johnson, K. (1991) *Enzymes 20* (in press).
Johnson, W. C., Jr. (1985) in *Methods of Biochemical analysis* (Glick, D., Ed.) pp 61–163, John Wiley & Sons, Inc., New York.
Knoop, F. (1904) *Beitr. Chem. Physiol. Pathol. 6*, 150.
Lau, S., Powell, P., Buettner, H., Ghisla, S., & Thorpe, C. (1986) *Biochemistry 25*, 4184–4189.
Lau, S., Brantely, R. K., & Thorpe, C. (1988) *Biochemistry 27*, 5089–5095.
Lau, S., Brantely, R. K., & Thorpe, C. (1989) *Biochemistry 28*, 8255–8262.
Lehman, T. C., Thorpe, C. (1990) *Biochemistry 29*, 10594–10601.
Lehman, T. C., Hale, D. E., Hhala, A., & Thorpe, C. (1990) *Anal. Biochem. 186*, 280–284.
McFarland, J. T., Lee, M., Reinsch, J., & Raven, W. (1982) *Biochemistry 21*, 1224–1229.
Powell, P. J., Lau, S., Killian, D., & Thorpe, C. (1987) *Biochemistry 26*, 3704–3710.
Schopfer, L. M., Massey, V., Ghisla, S., & Thorpe, C. (1988) *Biochemistry 27*, 6599–6611.
Schulz, H. (1991) *Biochim. Biophys. Acta 1081*, 109–120.
Srivastava, D. K., Smolen, P., Betts, G. F., Fukushima, T., Spivey, H. O., & Bernhard, S. A. (1989) *Proc. Natl. Acad. Sci. U.S.A. 86*, 6464–6468.
Steyn-Parvé, E. P., & Beinert, H. (1958) *J. Biol. Chem. 233*, 843–852.
Thorpe, C. (1981) *Methods Enzymol. 71*, 366–374.
Thorpe, C., Matthews, R. G., & Williams, C. H. (1979) *Biochemistry 18*, 331–337.
Thorpe, C., Ciardelli, T. L., Stewart, C. J., & Wieland, T. (1981) *Eur. J. Biochem. 118*, 279–282.
Wang, R., & Thorpe, C. (1991) *Biochemistry 30*, 7895–7901.